Automatic Hyperspectral Image Restoration Using Sparse and Low-Rank Modeling

Behnood Rasti, *Member, IEEE*, Magnus Orn Ulfarsson, *Member, IEEE*, and Pedram Ghamisi, *Member, IEEE*

***Abstract*— Hyperspectral restoration is a preprocessing step for hyperspectral imagery. In this letter, we propose a parameter-free method for the restoration of hyperspectral images (HSIs) called HyRes. The restoration method is based on a sparse low-rank model that uses the ℓ_1 penalized least squares for estimating the unknown signal. The Stein's unbiased risk estimator is exploited to select all the parameters of the model yielding a fully automatic (parameter free) technique. Experimental results confirm that HyRes outperforms the state-of-the-art techniques in terms of signal-to-noise ratio, structural similarity index, and spectral angle distance for a simulated data set and in terms of noise-level estimation for the real data sets used in this letter. In the experiments, it was noted that HyRes is computationally less expensive compared with competitive techniques. Therefore, HyRes can be used as a reliable automatic preprocessing step for further analysis of HSIs.**

***Index Terms*— Hyperspectral denoising, hyperspectral image (HSI), hyperspectral preprocessing, hyperspectral restoration (HyRes), low-rank and sparse modeling, mean square errors (MSEs), noise reduction, penalized least squares, Stein's unbiased risk estimator (SURE).**

I. Introduction

THE received radiance at the hyperspectral sensor is degraded by various sources such as atmospheric haze and instrumental noises. Atmospheric corrections are applied to compensate for the atmospheric effects. However, different types of noises exist in the digitized image such as thermal (Johnson) noise, quantization noise, and shot (photon) noise. The presence of noise could degrade the efficiency of the image analysis techniques. As a result, hyperspectral image (HSI) restoration can be considered as an important preprocessing step in HSI analysis [1], [2].

HSI restoration has considerably evolved in the past decade. The advantages of 3-D models, such as 3-D wavelets, over 2-D ones for HSI restoration have been explored in [3] and [4]. Some techniques have proposed spectral penalties for penalized least squares in order to consider spectral information [5]–[7]. A spatial–spectral prior for maximum *a posteriori* estimation was proposed in [8]. Cubic total variation (CTV) was developed in [9], which uses the spectral gradient to improve the restoration results compared with conventional TV denoising [10]. An adaptive CTV was suggested in [11], which preserves simultaneously both texture and edges.

Low-rank modeling has been found to be very useful for HSI restoration due to the redundancy along the spectral direction. Restoration techniques that exploit low-rank techniques have shown better performance than the ones that exploit full-rank models [2]. Tucker3 decomposition [12], which is a low-rank method, was used in [13] and [14] for HSI restoration. Also, a multidimensional Wiener filtering-based Tucker3 decomposition was suggested in [15]. Another low-rank method is the parallel factor analysis used in [16] for HSI restoration. In [17], a 3-D linear model and the ℓ_1 penalized least squares were used for HSI restoration. Additionally, a low-rank TV regularization was proposed for HSI in [18] and [2]. In [19], orthogonal TV component analysis was developed for HSI analysis. Wavelet-based sparse reduced-rank regression was proposed in [20] where a nonconvex optimization was exploited to estimate the unknown signal. In [21], a low-rank and sparse matrix decomposition was suggested for the restoration of HSI where the noise was assumed to be a mixture of Gaussian and a sparse distribution. This technique was further investigated by augmenting a total variation penalty to the restoration criterion in [22]. Noise-adjusted iterative low-rank matrix approximation was suggested in [23] to approximate the HSI with a low-rank matrix while considering the changes of the noise variance through the spectral bands. Also, weighted Schatten p-norm as a nonconvex low-rank regularizer was proposed in [24] for low-rank and sparse decomposition of HSI and was also used in [25] by exploiting a structure TV penalty to the minimization problem. Recently, a low-rank restoration technique was proposed in [26] where the low-rank constraint was applied on the spectral difference matrix.

Despite the considerable developments, HSI restoration techniques have usually not been used in HSI analysis as a preprocessing technique. This might be due to several reasons such as the computational costs, efficiency, reliability, and automation of the above-mentioned algorithms. The main goal of the restoration-based preprocessing stage is to improve the signal-to-noise ratio (SNR) of the observed data set. As a result, the presence of tuning parameters to be

Manuscript received August 12, 2017; revised September 22, 2017 and October 14, 2017; accepted October 15, 2017. Date of publication November 8, 2017; date of current version December 4, 2017. *(Corresponding author: Behnood Rasti.)*

B. Rasti is with the Keilir Institute of Technology , 235 Reykjavik, Iceland, and also with the Department of Electrical and Computer Engineering, University of Iceland, 101 Reykjavik, Iceland (e-mail: behnood@hi.is).

M. O. Ulfarsson is with the Department of Electrical and Computer Engineering, University of Iceland, 101 Reykjavik, Iceland (e-mail: mou@hi.is).

P. Ghamisi is with Deutsches Zentrum für Luft- und Raumfahrt (DLR) Earth Observation Center, Remote Sensing Technology Institute, SAR Signal Processing, Oberpfaffenhofen, 82234 Wessling, Germany (e-mail: pedram.ghamisi@dlr.de).

Color versions of one or more of the figures in this letter are available online at http://ieeexplore.ieee.org.

Digital Object Identifier 10.1109/LGRS.2017.2764059

set or selected by some *ad hoc* and/or experimental strategies makes the algorithm unreliable and problematic to be used as a preprocessing stage in HSI analysis. If the parameters were selected experimentally, they are extremely biased to the experiments and not guaranteed to be optimal for other data sets. Therefore, a reliable parameter selection technique based on statistical signal processing algorithms can considerably benefit a restoration technique.

In this letter, we propose a parameter-free hyperspectral restoration (HyRes) technique, which is suitable to be used as a preprocessing stage in HSI analysis. The hyperspectral signal is represented by a low-rank model and the estimation is done by using the ℓ_1 penalized least squares. Model parameter selection is a challenging task and it is of a great interest in real hyperspectral applications due to the absence of the original signal. Therefore, in the proposed technique, the parameters of the model have been selected by estimating the mean square error (MSE) yielding a parameter-free restoration technique. Hyperspectral Stein's unbiased risk estimator (HySURE) [27] is used for rank estimation and sparsity parameters are selected using Stein's unbiased risk estimator (SURE). In the experiments, the proposed method has been evaluated and compared with the state-of-the-art HSI restoration techniques based on image quality metrics such as SNR, the mean of the structural similarity (MSSIM) index, and the mean of spectral angle distance (MSAD). The experimental results confirm that HyRes outperforms the other techniques in terms of SNR, MSSIM, and MSAD in the case of simulated HSI and based on noise-level estimation in the case of real data sets used in this letter.

The rest of this letter is organized as follows. The proposed HyRes method is presented in Section II. SURE is given as a parameter selection method in Section III. The experimental results are given in Section IV, and Section V concludes this letter.

II. Hyperspectral Restoration

The notations used in this letter are as follows. The number of bands and pixels in each band are denoted by p and n, respectively. Matrices are represented by bold and capital letters, vectors by bold letters, and the element placed in the ith row and jth column of $\mathbf{A}$ by a_{ij}. $\hat{\mathbf{X}}$ stands for the estimate of $\mathbf{X}$ and $\|.\|_F$ is the Frobenius norm.

An HSI can be modeled by

$$\mathbf{H} = \mathbf{X} + \mathbf{N} \tag{1}$$

where $\mathbf{H}$ is an $n \times p$ matrix ($n = n_1 \times n_2$) containing the vectorized observed image at band i in its ith column, $\mathbf{X}$ is the true unknown signal that needs to be estimated, and $\mathbf{N}$ is an $n \times p$ matrix representing noise. The restoration task is to estimate the original (unknown) signal $\mathbf{X}$. Penalized (regularized) least squares is a common minimization framework used for the estimation in HSI restoration. It is composed of a fidelity term and a penalty term. The penalty term is often chosen based on the prior knowledge of the signal.

In [2], it was shown that capturing the spectral redundancy by low-rank modeling is more appropriate than full-rank modeling for HSI restoration. As a result, in [2], the HSI was modeled as

$$\mathbf{H} = \mathbf{A}\mathbf{W}_r\mathbf{M}_r^T + \mathbf{N} \tag{2}$$

where $\mathbf{A}$ ($n \times n$ matrix) represents 2-D wavelet basis, $\mathbf{M}_r$ is a $p \times r$ low-rank matrix containing the r-first spectral eigenvectors of the observed data $\mathbf{H}$, and $\mathbf{W}_r$ is an $n \times r$ matrix containing the corresponding coefficients for the unknown hyperspectral data, $\mathbf{X}$. The HSI is expected to be sparse in the 2-D wavelet basis. To enforce the sparsity, an ℓ_1 penalty on the wavelet coefficients $\mathbf{W}_r$ is used. Hence, the sparse restoration problem is given by

$$\hat{\mathbf{W}}_r = \arg\min_{\mathbf{W}_r} \frac{1}{2}\left\|\mathbf{H} - \mathbf{A}\mathbf{W}_r\mathbf{M}_r^T\right\|_F^2 + \sum_{t,k} \lambda_k |w_{tk}|. \tag{3}$$

Using trace properties and ignoring irrelevant terms, the minimization problem (3) can be simplified to

$$\arg\min_{\mathbf{W_r}} \frac{1}{2}\mathrm{tr}\left(\mathbf{W}_r^T\mathbf{W}_r\right) - \mathrm{tr}\left(\mathbf{B}\mathbf{W}_r^T\right) + \sum_{t,k} \lambda_k |w_{tk}| \tag{4}$$

where $\mathbf{B} = \mathbf{A}^T\mathbf{H}\mathbf{M}_r$. By adding the quadratic term $(1/2)\mathrm{tr}(\mathbf{B}^T\mathbf{B})$ (which is a constant), the minimization problem (4) can be rewritten as

$$\arg\min_{\mathbf{W_r}} \frac{1}{2}\|\mathbf{W}_r - \mathbf{B}\|_F^2 + \sum_{t,k} \lambda_k |w_{tk}|$$

which is a separable problem and can be solved pixelwise as

$$\arg\min_{w_{tk}} \frac{1}{2}(w_{tk} - b_{tk})^2 + \lambda_k |w_{tk}|. \tag{5}$$

Finally, it can be shown that the solution to (5) is given by the shrinkage function

$$\hat{w}_{tk} = \max(0, |b_{tk}| - \lambda_k)\frac{b_{tk}}{|b_{tk}|}. \tag{6}$$

Note that the hyperspectral signal is restored by $\hat{\mathbf{X}} = \mathbf{A}\hat{\mathbf{W}}_r\mathbf{M}_r^T$.

III. Automatic Parameters' Selection

In (3), λ_k and r are unknown variables and need to be estimated. λ_k is the sparsity tuning parameter and r is the rank number.

To estimate the rank, r, we use a rank estimation technique called HySURE [27]. HySURE also exploits models (1) and (2) to estimate the rank for HSIs using SURE. Note that HySURE assumes that $\lambda_1 = \lambda_2 =, \ldots, = \lambda_r = \lambda$, which decreases the complexity of the analysis due to the search range.

The HySURE formula (ignoring constants) is given by

$$\mathrm{HySURE}(r, \lambda_1, \ldots, \lambda_r) = \sum_{k=1}^{r}\sum_{t=1}^{n}\left(2I(|b_{tk}| > \lambda_k) - \max\left(0, b_{tk}^2 - \lambda_k^2\right)\right)$$

where $\mathbf{B} = [b_{tk}]$ and I is the indicator function.

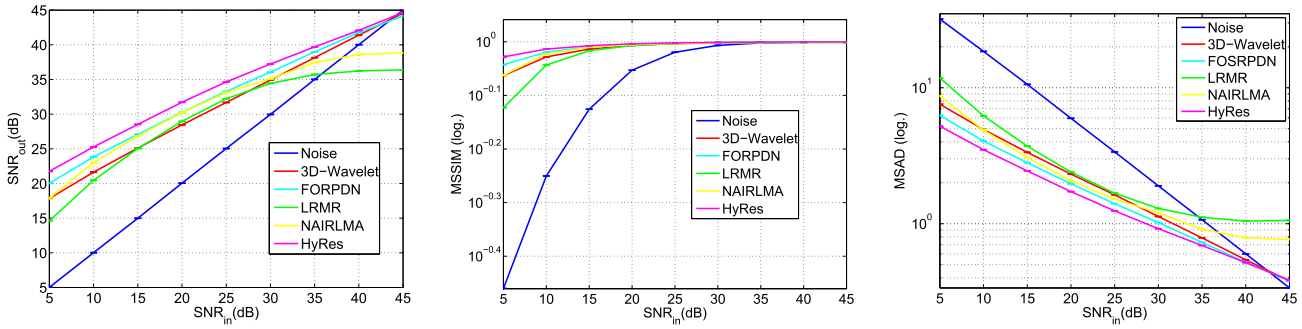

Fig. 1. Comparison of the performances for the studied HSI restoration methods applied on the simulated data set with respect to different levels of input Gaussian noise. (a) SNR_{out} (dB). (b) MSSIM (logarithmic scale). (c) MSAD (logarithmic scale).

IV. Experimental Results

In experiments, we compare HyRes with 3-D wavelet modeling (3-D Wavelet) [3], first-order spectral roughness penalty denoising (FORPDN) [6], low-rank matrix recovery (LRMR) [21], and noise-adjusted iterative low-rank matrix approximation (NAILRMA) [23]. The experiments are conducted on a noisy simulated HSI and real data sets.

A. Simulated Noisy Data Set

For the simulated noisy data set, we use the Pavia university data. The data were collected by ROSIS-03 with 1.3-m spatial resolution per pixel and are composed of 610 × 340 pixels in 103 bands. In this section, the experiments are applied on a portion (128 × 128 × 96) of the Pavia university data set where the variance of the Gaussian noise added varies along the spectral axis (σ_i^2) according to

$$\sigma_i^2 = \sigma^2 \frac{e^{-\frac{(i-d/2)^2}{2\eta^2}}}{\sum_{j=1}^{d} e^{-\frac{(j-d/2)^2}{2\eta^2}}}$$

where the power of the noise is controlled by σ and η behaves like the standard deviation for the Gaussian bell curve [28]. To evaluate the restoration results for the simulated data set, SNR and MSAD are used. The output SNR in decibels is given by

$$\text{SNR}_{\text{out}} = 10\ \log_{10}\left(\|\mathbf{X}\|_F^2 / \|\mathbf{X} - \hat{\mathbf{X}}\|_F^2\right)$$

and the input SNR in decibels is given by

$$\text{SNR}_{\text{in}} = 10\ \log_{10}\left(\|\mathbf{X}\|_F^2 / \|\mathbf{X} - \mathbf{H}\|_F^2\right).$$

To evaluate the presence of artifacts in the restored image, we also use the structural similarity (SSIM) index [29] for the whole data cube that is based on the similarity with a reference image as

$$\text{SSIM}(\mathbf{X}, \hat{\mathbf{X}}) = \frac{(2\mu_{\mathbf{X}}\mu_{\hat{\mathbf{X}}} + C_1)(2\sigma_{\mathbf{X}\hat{\mathbf{X}}} + C_2)}{(\mu_{\mathbf{X}}^2 + \mu_{\hat{\mathbf{X}}}^2 + C_1)(\sigma_{\mathbf{X}}^2 + \sigma_{\hat{\mathbf{X}}}^2 + C_2)}$$

where $\mu_{\mathbf{X}}$, $\mu_{\hat{\mathbf{X}}}$, $\sigma_{\mathbf{X}}$, and $\sigma_{\hat{\mathbf{X}}}$ denote mean values and standard deviations for the reference image, $\mathbf{X}$, and the denoised image, $\hat{\mathbf{X}}$. $\sigma_{\mathbf{X}\hat{\mathbf{X}}}$ indicates the cross covariance between the two images. $C_1 = (K_1 M)^2$ and $C_2 = (K_2 M)^2$ are constants to avoid the unstable situation that happens when $\mu_{\mathbf{X}}^2 + \mu_{\hat{\mathbf{X}}}^2$ or $\sigma_{\mathbf{X}}^2 + \sigma_{\hat{\mathbf{X}}}^2$ is close to zero. K_1 and K_2 are small constants ($K_1, K_2 \ll 1$) and M is the dynamic range of the image. In this letter, K_1 and K_2 are set to 0.01 and 0.03, respectively (these are the default values) and $M = 255$. SSIM is between 0 and 1, where 1 reveals the situation that the two images are the same. Here, we use the mean of SSIM (MSSIM) as an SSIM index for the whole data cube.

Fig. 1(a) shows the comparison of the HSI restoration techniques based on SNR. SNR_{in} is the level of the noise added (in decibels) to the simulated data set and SNR_{out} shows the level of the reconstructed signal compared with the input noise. The results are shown when SNR_{in} varies from 5 to 45 dB with the increments of 5 dB.

In Fig. 1(a), the blue line shows the noise levels, and therefore, the performance of the HSI restoration methods is compared with respect to the noise levels. As can be seen, 3-D wavelet, FORPDN, and HyRes demonstrate consistency with respect to the level of noise power. On the other hand, restoration gains obtained using LRMR when $\text{SNR}_{\text{in}} \leq 15$ dB and $\text{SNR}_{\text{in}} \geq 30$ dB are not satisfactory. A similar trend can be observed in the performance of NAIRLMA; however, the gains are improved compared with LRMR. Also, it can be seen that FORPDN, which is based on 2-D wavelet and the FORPDN penalty, outperforms 3-D wavelet restoration, which confirms the importance of the spectral correlations for HSI restoration. The results demonstrate that HyRes, which exploits on low-rank and sparse modeling, outperforms the other techniques used in this experiment based on SNR.

Fig. 1(b) and (c) compare the HSI restoration techniques in terms of MSSIM and MSAD with respect to the input noise power, respectively. The results are shown in logarithmic scale for a better visual representation. The results follow the trend of SNR_{out}, and it can be seen that HyRes outperforms the other techniques also based on MSSIM and MSAD. All the results depicted in this section are over ten experiments (adding random Gaussian noise) and the error bars show the standard deviations.

Note that Wavelab Fast (a fast wavelet toolbox developed for HSI analysis) [30] was used for the implementation of Wavelet transforms. For all the experiments performed in this letter,

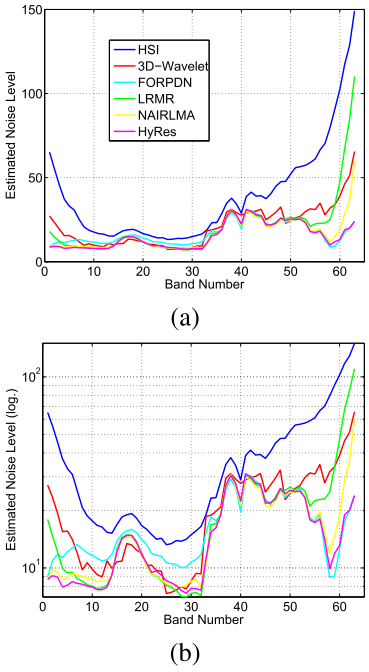

Fig. 2. (a) Comparison of the performances for different HSI restoration methods applied on Trento based on the estimation of the standard deviation of the noise in the spectral bands. (b) Comparison is shown in logarithmic scale.

TABLE I

ESTIMATION OF THE NOISE STANDARD DEVIATION IN THE RESTORED HSIS

	HSI	3D Wavelet	FORPDN	LRMR	NAILRMA	HyRes
Trento	38.87	21.06	16.65	20.40	16.54	**15.35**
Indian Pines	10.26	5.71	4.65	4.12	4.194	**3.86**

Daubechies wavelets were used with two and ten coefficients for spectral and spatial bases, respectively. Five decomposition levels were used for the filter banks.

B. Real Data Sets

Here, we use two real data sets to validate the performance of the proposed approach. The first data set was captured over a rural area in the south of the city of Trento, Italy. It is composed of 600 × 166 pixels with a spatial resolution of 1 m. The spectral range begins from 402.89 to 989.09 nm in 63 bands. We also use the Indian Pines data set composed of 145 × 145 pixels in 220 bands. Indian Pines is a widely used HSI in the restoration literature and it was captured by the airborne hyperspectral sensor AVIRIS with 20-m spatial resolution per pixel and 10-nm spectral resolution per band.

To compare the performance of the restoration techniques, we use the patchwise noise-level estimation given in [31], which selects patches from the noisy image to estimate the noise level using principal component analysis. Fig. 2(a) shows the estimated standard deviation of the noise with respect to the band numbers before and after applying the restoration techniques on the Trento data set. The blue line indicates the noise level in each band. Also, the same comparison in logarithmic scale is given in Fig. 2(b) to have a better demonstration. As can be seen, HyRes displays more consistency in noise removal throughout the bands than the other techniques.

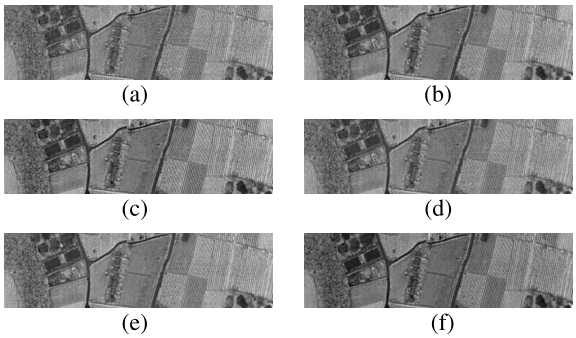

Fig. 3. Visual comparison of the performances of the HSI restoration methods applied on the Trento data set. (a) Band 63. (b) 3-D Wavelet. (c) FORPDN. (d) LRMR. (e) 3-D NAILRMA. (f) HyRes.

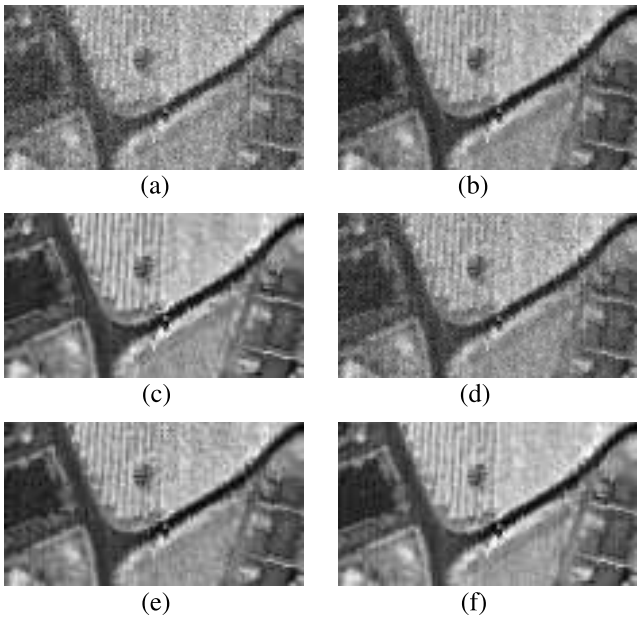

Fig. 4. Performances of the HSI restoration methods applied on the selected area of the Trento data set. (a) Band 63. (b) 3-D Wavelet. (c) FORPDN. (d) LRMR. (e) 3-D NAILRMA. (f) HyRes.

The noise levels in first few bands as well as the last few bands after using 3-D wavelet and LRMR restoration are high. FORPDN gives the highest noise level for the bands from 6 to 32. Also, the last couple of bands contain high noise level in the case of using NAIRLMA. The overall noise level estimated after using different HSI restoration techniques is given in Table I for both Trento and Indian Pines. It can be seen that HyRes gives the lowest overall noise level among the other techniques. A visual comparison of the restored band 63 from the Trento data set is depicted in Fig. 3. Fig. 4 compares the results of the selected area of the Trento data. It can be seen that FORPDN and HyRes show better visual performance than the other techniques.

Table II compares the CPU processing time in seconds for different restoration approaches used in the experiment. The results shown confirm that HyRes is computationally less expensive than the other HSI restoration techniques. Moreover, FORPDN is a computationally efficient technique. On the other hand, LRMR takes the highest CPU processing time. All the experiments in this section have been done in MATLAB on a computer having an Intel Core i7-4710HQ

TABLE II
CPU PROCESSING TIME IN SECONDS FOR DIFFERENT RESTORATION APPROACHES USED IN THE EXPERIMENT

	3D Wavelet	FORPDN	LRMR	NAILRMA	HyRes
Trento	8.26	3.70	102.05	19.41	**3.34**
Indian Pines	6.74	3.72	67.24	10.07	**1.96**

CPU at 2.5 GHz, 12 GB of memory, and 64-b operating system.

V. CONCLUSION

In this letter, a sparse and low-rank modeling and restoration method called HyRes was proposed for HSIs. HySURE and SURE were exploited to select rank and sparsity parameters of the model based on the estimate of MSE, which led to an automatic (parameter-free) restoration technique. The proposed technique was compared with the state-of-the-art techniques. Experiments were performed on simulated and real data sets. Experimental results confirm that HyRes outperforms the other techniques used in the experiments in terms of SNR, MSSIM, and MSAD for the simulated data set. In the case of the real data sets, the HSI restoration techniques were compared based on the noise level estimated from the restored HSI. The real data experiments were performed on Trento and Indian Pines data sets. The results confirm that the restored HSIs obtained using HyRes contain less noise level compared with the ones obtained using competitive techniques. Moreover, visual comparison showed that HyRes together with FORPDN outperforms the other restoration methods visually. Furthermore, it has been demonstrated that the proposed method is computationally less expensive than the competitive methods, and therefore, it has a high potential to be exploited as a restoration-based preprocessing step for further HSI analysis.

ACKNOWLEDGMENT

The authors would like to thank Prof. L. Bruzzone of the University of Trento and Prof. P. Gamba of the University of Pavia for providing the Trento and Pavia data sets, respectively.

REFERENCES

[1] D. A. Landgrebe and E. Malaret, "Noise in remote-sensing systems: The effect on classification error," *IEEE Trans. Geosci. Remote Sens.*, vol. GE-24, no. 2, pp. 294–300, Mar. 1986.

[2] B. Rasti, "Sparse hyperspectral image modeling and restoration," Ph.D. dissertation, Dept. Elect. Comput. Eng., Univ. Iceland, Reykjavik, Iceland, Dec. 2014.

[3] B. Rasti, J. R. Sveinsson, M. O. Ulfarsson, and J. A. Benediktsson, "Hyperspectral image denoising using 3D wavelets," in *Proc. IEEE IGARSS*, Jul. 2012, pp. 1349–1352.

[4] B. Rasti, J. R. Sveinsson, and M. O. Ulfarsson, "Sure based model selection for hyperspectral imaging," in *Proc. IEEE IGARSS*, Jul. 2014, pp. 4636–4639.

[5] A. Zelinski and V. Goyal, "Denoising hyperspectral imagery and recovering junk bands using wavelets and sparse approximation," in *Proc. IEEE IGARSS*, Aug. 2006, pp. 387–390.

[6] B. Rasti, J. R. Sveinsson, M. O. Ulfarsson, and J. A. Benediktsson, "Hyperspectral image denoising using first order spectral roughness penalty in wavelet domain," *IEEE J. Sel. Topics Appl. Earth Observ. Remote Sens.*, vol. 7, no. 6, pp. 2458–2467, Jun. 2014.

[7] B. Rasti, J. R. Sveinsson, M. O. Ulfarsson, and J. A. Benediktsson, "Wavelet based hyperspectral image restoration using spatial and spectral penalties," *Proc. SPIE*, vol. 8892, pp. 8892-1–8892-8, 2013. [Online]. Available: http://dx.doi.org/10.1117/12.2029257, doi: 10.1117/12.2029257.

[8] S.-L. Chen, X.-Y. Hu, and S.-L. Peng, "Hyperspectral imagery denoising using a spatial-spectral domain mixing prior," *J. Comput. Sci. Technol.*, vol. 27, no. 4, pp. 851–861, 2012.

[9] H. Zhang, "Hyperspectral image denoising with cubic total variation model," *ISPRS Ann. Photogramm., Remote Sens. Spatial Inf. Sci.*, vol. 7, pp. 95–98, Jul. 2012.

[10] L. I. Rudin, S. Osher, and E. Fatemi, "Nonlinear total variation based noise removal algorithms," *Phys. D, Nonlinear Phenomena*, vol. 60, nos. 1–4, pp. 259–268, 1992.

[11] Q. Yuan, L. Zhang, and H. Shen, "Hyperspectral image denoising employing a spectral–spatial adaptive total variation model," *IEEE Trans. Geosci. Remote Sens.*, vol. 50, no. 10, pp. 3660–3677, 2012.

[12] L. R. Tucker, "Some mathematical notes on three-mode factor analysis," *Psychometrika*, vol. 31, no. 3, pp. 279–311, 1966.

[13] L. D. Lathauwer, B. D. Moor, and J. Vandewalle, "On the best rank-1 and rank-(R_1, R_2, ..., R_N) approximation of higher-order tensors," *SIAM J. Matrix Anal. Appl.*, vol. 21, no. 4, pp. 1324–1342, Mar. 2000.

[14] N. Renard, S. Bourennane, and J. Blanc-Talon, "Denoising and dimensionality reduction using multilinear tools for hyperspectral images," *IEEE Geosci. Remote Sens. Lett.*, vol. 5, no. 2, pp. 138–142, Apr. 2008.

[15] D. Letexier and S. Bourennane, "Noise removal from hyperspectral images by multidimensional filtering," *IEEE Trans. Geosci. Remote Sens.*, vol. 46, no. 7, pp. 2061–2069, Jul. 2008.

[16] X. Liu, S. Bourennane, and C. Fossati, "Denoising of hyperspectral images using the parafac model and statistical performance analysis," *IEEE Trans. Geos. Remote Sens*, vol. 50, no. 10, pp. 3717–3724, Oct. 2012.

[17] B. Rasti, J. R. Sveinsson, M. O. Ulfarsson, and J. A. Benediktsson, "Hyperspectral image denoising using a new linear model and sparse regularization," in *Proc. IEEE IGARSS*, Jul. 2013, pp. 457–460.

[18] B. Rasti, J. R. Sveinsson, and M. O. Ulfarsson, "Total variation based hyperspectral feature extraction," in *Proc. IEEE IGARSS*, Jul. 2014, pp. 4644–4647.

[19] B. Rasti, M. O. Ulfarsson, and J. R. Sveinsson, "Hyperspectral feature extraction using total variation component analysis," *IEEE Trans. Geosci. Remote Sens.*, vol. 54, no. 12, pp. 6976–6985, Dec. 2016.

[20] B. Rasti, J. R. Sveinsson, and M. O. Ulfarsson, "Wavelet-based sparse reduced-rank regression for hyperspectral image restoration," *IEEE Trans. Geosci. Remote Sens.*, vol. 52, no. 10, pp. 6688–6698, Oct. 2014.

[21] H. Zhang, W. He, L. Zhang, H. Shen, and Q. Yuan, "Hyperspectral image restoration using low-rank matrix recovery," *IEEE Trans. Geosci. Remote Sens.*, vol. 52, no. 8, pp. 4729–4743, Aug. 2014.

[22] W. He, H. Zhang, L. Zhang, and H. Shen, "Total-variation-regularized low-rank matrix factorization for hyperspectral image restoration," *IEEE Trans. Geosci. Remote Sens.*, vol. 54, no. 1, pp. 178–188, Jan. 2016.

[23] W. He, H. Zhang, L. Zhang, and H. Shen, "Hyperspectral image denoising via noise-adjusted iterative low-rank matrix approximation," *IEEE J. Sel. Topics Appl. Earth Observ. Remote Sens.*, vol. 8, no. 6, pp. 3050–3061, Jun. 2015.

[24] Y. Xie, Y. Qu, D. Tao, W. Wu, Q. Yuan, and W. Zhang, "Hyperspectral image restoration via iteratively regularized weighted schatten p-norm minimization," *IEEE Trans. Geosci. Remote Sens.*, vol. 54, no. 8, pp. 4642–4659, Aug. 2016.

[25] Z. Wu, Q. Wang, J. Jin, and Y. Shen, "Structure tensor total variation-regularized weighted nuclear norm minimization for hyperspectral image mixed denoising," *Signal Process.*, vol. 131, pp. 202–219, Feb. 2017. [Online]. Available: http://www.sciencedirect.com/science/article/pii/S0165168416301827

[26] L. Sun, B. Jeon, Y. Zheng, and Z. Wu, "Hyperspectral image restoration using low-rank representation on spectral difference image," *IEEE Geosci. Remote Sens. Lett.*, vol. 14, no. 7, pp. 1151–1155, Jul. 2017.

[27] B. Rasti, M. O. Ulfarsson, and J. R. Sveinsson, "Hyperspectral subspace identification using sure," *IEEE Geosci. Remote Sens. Lett.*, vol. 12, no. 12, pp. 2481–2485, Dec. 2015.

[28] J. M. Bioucas-Dias and J. M. P. Nascimento, "Hyperspectral subspace identification," *IEEE Trans. Geosci. Remote Sensing*, vol. 46, no. 8, pp. 2435–2445, Aug. 2008.

[29] Z. Wang, A. C. Bovik, H. R. Sheikh, and E. P. Simoncelli, "Image quality assessment: From error visibility to structural similarity," *IEEE Trans. Image Process.*, vol. 13, no. 4, pp. 600–612, Apr. 2004.

[30] B. Rasti. (May 2016). *Wavelab Fast*. [Online]. Available: https://www.researchgate.net/publication/303445667_Wavelab_fast

[31] X. Liu, M. Tanaka, and M. Okutomi, "Noise level estimation using weak textured patches of a single noisy image," in *Proc. 19th IEEE Int. Conf. Image Process. (ICIP)*, Sep. 2012, pp. 665–668.